BABEŞ-BOLYAI UNIVERSITY CLUJ-NAPOCA
FACULTY OF PHYISICS
BIOPHYSICS AND MEDICAL PHYSICS

DISSERTATION THESIS

Scientific Coordinators:
Prof. Dr. Nicolae Leopold
Dr. Iancu D. Ștefania

Student:
Chiș Alexandru-Ștefan

2023

Babeş-Bolyai University Cluj-Napoca
Faculty of physics
Biophysics and Medical Physics

Dissertation thesis

Silver Nanogrid Solid Substrates for SERS bioanalysis

Scientific Coordinators:
Prof. Dr. Nicolae Leopold
Dr. Iancu D. Ștefania

Student:
Chiș Alexandru-Ștefan

2023

Contents

Abstract

This theisis presents a silver nanogrids (AgNGs) solid substrate which allows surface-enchanced Raman spectroscopy (SERS) spectra acquisition of serum without the need for deproteination. Silver and gold nanoparticles are commonly used as SERS substrates, but they have limitations in reproducibility and are affected by the presence of proteins. A stop-and-go convective self-assembly method was used to prepare the AgNGs. The distance between AgNGs wires was optimized using Nile Blue (NB) as a test molecule. Furthermore, the optimal substrate reached a limit of detection for NB of 10^{-9} M and a 5.8% variation of NB SERS signal between substrates. Finally, the AgNGs substrate was tested with real-life canine and human serum samples. The results of this thesis show that an AgNGs substrate can be employed with real-life serum samples bypassing the deproteinization step, thereby facilitationg easier and faster acquisition of SERS spectra and advancing the implementation of SERS techinique in clinical diagnosis.

Introduction

Surface-enhanced Raman spectroscopy (SERS) is a promising analytical technique that has recently generated significant attention in the field of clinical diagnostics [1]. Its ease of use, fast analysis time, and exceptional sensitivity make an attractive tool for both disease screening and diagnosis. SERS has demonstrated its remarkable performance as an emerging approach, in numerous studies [2–5], and support tool [6, 7] for various diseases (e.g. cancer, Alzheimer, traumatic brain injury). However, its implementation in the clinical setting is hampered by the lack of a standardized operating procedure, which poses a major challenge to its successful translation. Therefore, the development of a universal protocol for SERS implementation in clinical diagnostics is essential to harness the full potential of this innovative analytical technique.

In the field of studies exploring the potential clinical applications of SERS, colloidal solutions of silver or gold have become the substrates of choice [2, 4, 6, 8], due to their facile preparation and the ease with which physico-chemical parameters such as form and dimensions can be modified as you need. However, while colloidal nanoparticles are convenient, solid substrates are known to improve the reproducibility of SERS measurements [9–11]. Additionally, when attempting to obtain SERS spectra of serum using colloidal nanoparticles, proteins can form a protein corona on the surface of the nanoparticles, which can obstruct other molecules from adsorbing onto the metallic surface. Consequently, no SERS signal can be detected (except proteins SERS spectrum), since SERS is only capable of detecting molecules that adsorb to the metallic substrate [12]. To overcome this challenge, proteins must be removed prior to the SERS analysis step, which dilutes the sample and prolongs the processing time of the sample.

This study presents a novel solid silver substrate in the form of silver nanogrids (AgNGs) which enables the acquisition of SERS spectra of serum samples, without the need for serum deproteinization. AgNGs were fabricated using the stop-and-go convective self-assembly (SG-CSA) method, which is a facile and rapid technique. The CSA method utilizes the movement of a meniscus between a liquid and a solid to create organized structures. The deposition process involves placing a droplet of colloidal suspension on a substrate, followed by the evaporation of the liquid in the droplet. As the meniscus moves across the substrate, the particles in the colloidal

solution are deposited along the meniscus due to the movement caused by the solvent evaporation [13, 14].

The spacing between the lines of AgNG was optimized to obtain the highest SERS signal. The sensitivity and reproducibility of the substrate were evaluated using Nile Blue. Subsequently, the substrate was tested on serum samples, revealing that the SERS spectrum of purine metabolites can be detected even in the presence of proteins. Conversely, for colloidal solutions, no SERS spectrum was obtained under the same conditions.

In conclusion, an optimized substrate of AgNGs has been developed which can be utilized for measuring SERS spectra of real-life samples, bypassing the need for deproteinization. This advancement has significant implications for clinical diagnostics and biomedical research.

In the first chapter of this study, a brief overview of SERS spectroscopy was presented, including its fundamental concepts and the two theories that sustain the approach. Furthermore, the use of SERS spectroscopy in the biomedical field, as demonstrated in recent studies, was discussed in relation to biofluids.

The second chapter outlines the experimental methods and materials utilized for acquiring SERS spectra, processing the resulting data, and preparing the solutions required for this study.

Finally, the third chapter discusses the findings of this investigation, which include the optimization of AgNGs substrate parameters and a comparison of AgNG and colloidal AgNP substrates with respect to various biofluids.

Chapter 1. Theoretical concept

1.1. Surface Enchanced Raman-Scattering (SERS)

All matter is made up of molecules that can exist in solid, liquid, or gas phases. Chemical bonds within molecules result in non-uniform charge distribution, leading to the formation of dipoles. Remarkably, light can alter the charge distribution within molecules, thereby creating or changing dipole moments. This results in the formation of an oscillating dipole, which generates an electromagnetic field. The interaction of the incident light waves with the charge distribution within the molecule can provide valuable qualitative and quantitative insights into its molecular composition. It's important to note that this interaction is unique to each molecule.[15]

Raman spectroscopy is a useful analytical tool due to its strong correlation between signal and concentration, as well as its ease of acquisition. However, a major drawback of this technique is its low sensitivity, which makes it difficult to acquire spectra from biological samples with low substance concentrations. To address this problem, Surface-Enhanced Raman Scattering (SERS) can be used, which can analyze samples even at micro or nano-molar concentrations.

SERS is achieved by enhancing Raman signals through two mechanism: first, by placing the molecule in the enahcend electromagnetic field generated by the interaction of the surface plasmons of a metallic substrate with the incident light; and second, by a charge transfer between the metallic substrate and the molecule that is adsorbed onto it, However, two questions arise: can all molecules be brought close to the metal substrate, and is the resulting SERS signal strong enough to be observed? While attaching molecules to the substrate is generally possible, it requires chemical manipulation and is not always easy. Obtaining a detectable signal is easy with regular Raman scattering but can be challenging when weaker signals are involved. To observe the signal, it all comes down to optimizing various parameters to maximize enhancement, surface area, the number of absorbed molecules, and the optical mechanism used. [16]

SERS was first observed by Fleischman in 1970 and later explained by Jeanmarie and Van Duyne, as well as Albert and Creighton in 1977. The effect is described by two theories: electromagnetic

and chemical. Both are accepted by the SERS community, with the electromagnetic effect leading to significantly higher amplifications than the chemical effect. When a metal sphere is excited, plasmon oscillations occur, which are collective oscillations of free electrons in ionic metals. In particles smaller than the wavelength of the excitation light, these oscillations are enhanced, which leads to the SERS effect.[17]

1.2. The Electromagnetic Theory

The oscillation of surface plasmons on an isolated metal sphere is supported by collective oscillations of free electrons in ionic metals. When particles smaller than the wavelength used are considered, they are called dipolar plasmons. The more free the electrons are in the metal particles, the more resonant the dipolar plasmons become. By exciting the small particles with a resonant laser, they emit radiation.

The radiation emitted by dipolar plasmons is a process correlated with the exciting field and is characterized by the spatial distribution of the electromagnetic field. In some regions, the radiation intensity is zero, while in others, close to the metal surface, the light intensity is much higher.

The problem is simplified by considering the polarizability of the Raman tensor and a polarized field along a flat surface (z-axis), which makes the problem one-dimensional. The induced dipole moment in the molecule by the incident field and the image field is given by the equation:

$$\mu = \alpha(E + E_{im}), \tag{1}$$

where E and E_{im} are the incident field and the image field, and α is a z-axis component of the molecular polarizability. E_{im} is defined by the formula:

$$E_{im} = \frac{\left[\frac{\varepsilon-\varepsilon_0}{\varepsilon+\varepsilon_0}\right]\mu}{4r^3} \ , \tag{2}$$

where r is the distance between the dipole and surface. By rearranging equation (1) and replacing E_im from equation (2), we obtain:

$$\mu = \alpha\left[1 - \frac{\left(\frac{\alpha}{4r^3}\right)(\varepsilon-\varepsilon_0)}{\varepsilon+\varepsilon_0}\right]^{-1} E \quad , \tag{3}$$

which represents a conventional expression for the induced dipole moment by the electric field E. However, instead of the polarizability α, it has an effective polarizability:

$$\alpha_{eff} = \frac{\alpha}{1-(\alpha/4r^3)(\varepsilon-\varepsilon_0)/(\varepsilon+\varepsilon_0)}, \quad (4)$$

which has a limit equal to 1, corresponding to the excitation of surface plasmons in metals at a frequency where Re(ε)= -ε0.[18]

Using reasonable parameters, it can be demonstrated that for silver, Raman enhancement in excess of 10^6 is possible at r=1.65Å or even smaller. The Raman enhancement is a characteristic of the substrate and does not depend on the target molecule. It can reach values up to 10^{10} and occurs as a result of the localization of light on the substrate surface, specifically the coupling of photons with surface electrons. The collective vibration of these electrons in the upper layers of the metallic nanostructure is called plasmon. If the incident laser radiation meets the plasmonic resonance condition, an intense electromagnetic field will be generated by the collective movement of surface plasmons. (Figure 1.1).

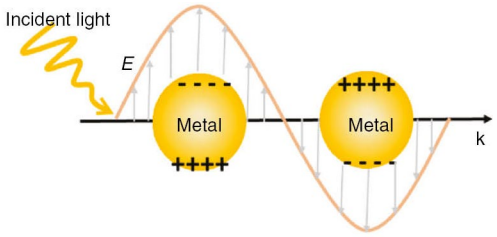

***Figure 1.1**. Surface plasmon resonance. [19]*

The molecule must be in the vicinity of the nanostructure, specifically in the action zone of the electromagnetic field generated by the plasmonic vibration raging between 1 and 10 nm. In the nanoworld, this effect is considered a long-range action effect (compared to a chemical bond). [20]

The electromagnetic field generated around the nanostructure as a result of the excitation of surface plasmons with laser radiation will modify the efficiency of Raman scattering because the scattered radiation power of a dipole depends on the medium in which it is located.

1.3. The Chemical Effect

The underlying mechanism of the SERS effect involves a complex physicochemical interaction between the molecule and the metal substrate. The extent of this interaction depends on the energy levels and characteristics of the molecule being analyzed, and typically occurs at distances of a few Angstroms between the molecule and substrate. Two distinct modes of interaction between the molecule and substrate have been identified: physisorption and chemisorption.

Physisorption refers to a relatively weak, non-chemical van der Waals interaction between the molecule and the metallic substrate. This mode of interaction does not typically result in significant changes to the energy levels of the molecule.

Chemisorption, on the other hand, involves the formation of a molecule-metal assembly through the hybridization of the metal and molecular orbitals of the absorbent. This results in the formation of bonding and antibonding states that can facilitate resonant electronic transfer between the highest occupied molecular orbitals (HOMO) and lowest unoccupied molecular orbitals (LUMO) of the metal-adsorbate complex. The SERS effect is thought to arise from this resonant electronic transfer.[21–23]

From a chemical perspective, the SERS effect is explained as a charge transfer between the metal surface and the analyzed molecule, which only occurs when the molecule is absorbed on the metal surface. One notable demonstration of this effect is that the electrode potential at which the SERS intensity is maximum is dependent on the energy of the incident laser. The potential at which the SERS intensity is maximum can either increase (as in the case of charge transfer from absorbed metal to molecule, such as in the Ag-pyridine system) or decrease (as in the case of charge transfer from absorbed molecule to metal, such as in the Ag-piperidine system) with increasing laser intensity. This is shown in Figure 1.2, where the pyridine band increases with increasing electron energy while the piperidine band decreases with increasing energy.

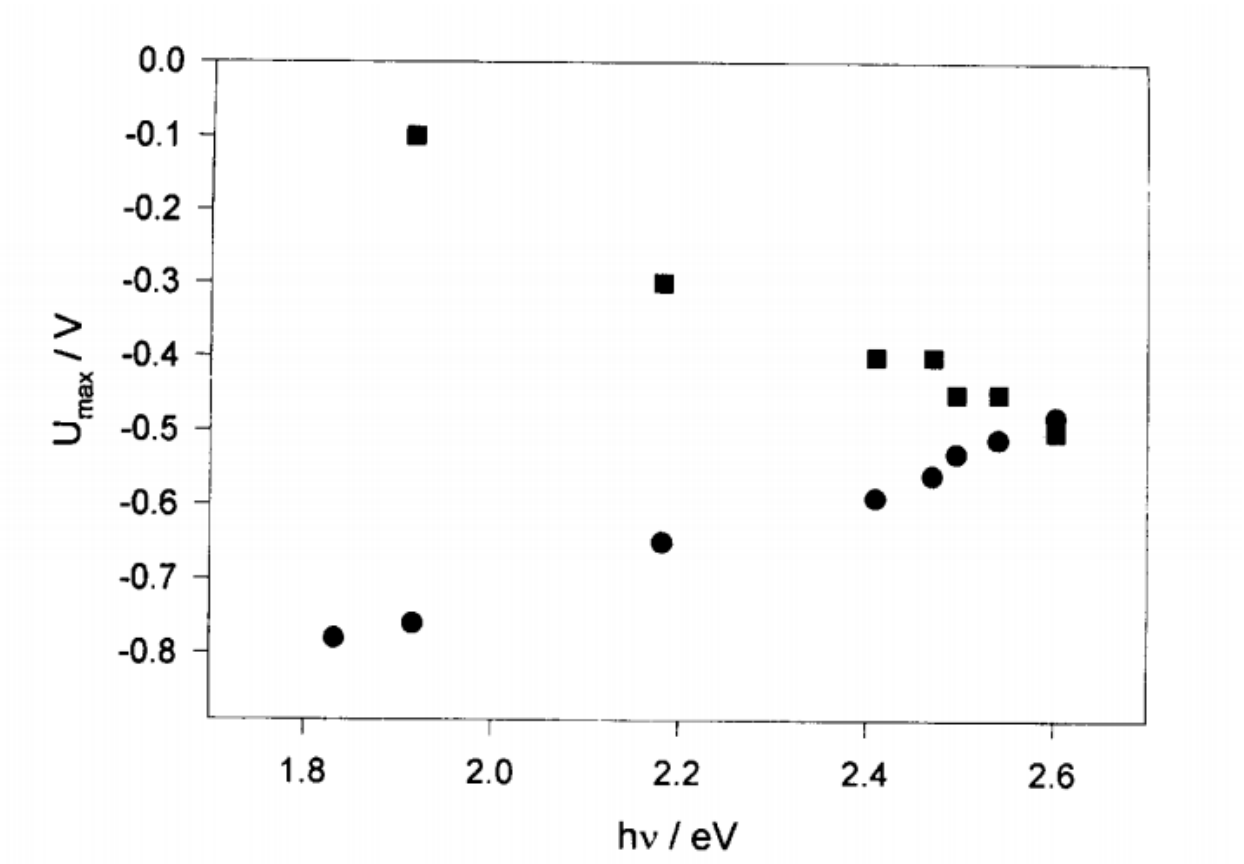

Figure 1.2 *Electrode potential at maximum SERS intensity is observed (U_{max}) as an energy function of the proton (hν). The black dot is pyridine band adsorbed on Ag (1018 cm^{-1}), and with black square is piperidine band absorbed on Ag (1007 cm^{-1})[24]*

1.4. Biofluids

Biofluids are complex fluids that are found in our body such as blood, urine, saliva, and cerebrospinal fluid. They serve as vital carriers of biomolecules and provide valuable information about an organism physiological state. Analyzing the composition of biofluids is of great significance in clinical and research settings, as it offers insights into disease diagnosis, therapeutic monitoring, and understanding biological processes.[6, 25, 26].

Proteins, present in human blood, mostly in high concentrations, they can adhere to the nanoparticle surfaces and form a layer that interferes with the Raman signal. This layer of proteins may act as a

barrier, hindering the direct interaction between the target analyte molecules and the SERS-active surface. As a result, the signal enhancement provided by the SERS substrate may be reduced or even lost, leading to a decrease in the sensitivity and accuracy of the measurements.[27]

Purine metabolites are a group of molecules derived from the purine nucleotides metabolism by breaking down the DNA or RNA. Some common purine metabolites are Xanthine, Hypoxanthine, Uric acid, Adenine, Guanine. SERS is a good way of detecting these purine metabolites from various biofluds such as urine, blood serum and saliva. Figure 1.3 is showing a simplified representation of purine metabolism pathway from DNA to Uric acid.

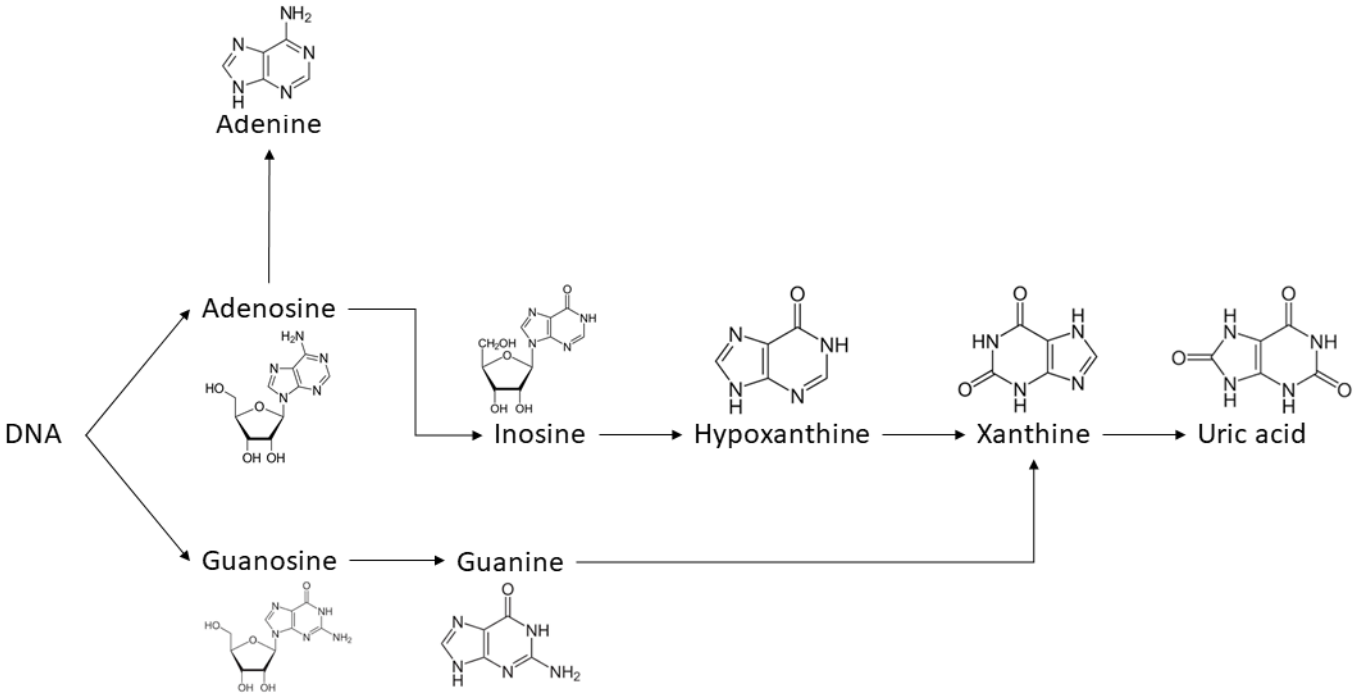

Figure 1.3 Representation of purine metabolism pathway.

Abnormal serum uric acid levels play a crucial role in the diagnostic assessment of certain kidney diseases, namely hyperuricemia and hypouricemia. Moreover, the identification of enzymatic defects in purine metabolism allows for the diagnosis of gout, a condition characterized by impaired purine metabolism. Emerging evidence indicates that uric acid may also serve as a significant factor in the pathogenesis of chronic kidney diseases.[28]

Chapter 2. Materials and Methods

2.1. Silver nanogrids synthesis

To obtain a regular morphology of the substrate, which can be easily reproduced, the nanoparticles were not air-dried in the form of a drop.

AgNGs were fabricated via the stop-and-go convective self-assembly (SG-CSA) method, starting with the synthesis of citrate-reduced silver nanoparticles (cit-AgNPs) using the Lee-Meisel method [29]. The resulting cit-AgNP solution was concentrated via centrifugation at 7300 g for 10 minutes, yielding a precipitate that was subsequently utilized. A 2 µl drop of the concentrated cit-AgNPs was then placed at a 40° angle between two slides, and the meniscus of the drop was translated across the substrate. After 0.25 mm of movement, the meniscus was intentionally halted for 7 seconds, allowing a line of nanoparticles to deposit due to solvent evaporation. This stop-and-go process was repeated 32 times, generating 32 wires of silver nanoparticles (AgNWs). The substrate comprising the 32 AgNWs was then positioned perpendicularly on a motorized stage, and the SG-CSA procedure was repeated after 15 minutes. Figure 2.1 provides a visual representation of the stepwise procedure employed for the synthesis of the AgNGs. Notably, the SG-CSA system employed in this study was a custom-made set-up that included a motorized translation stage (Thorlabs KMTS50 E/M) with a speed of 1mm/s, which ensured that no additional nanoparticle assemblies were formed during the meniscus translation across the slide.

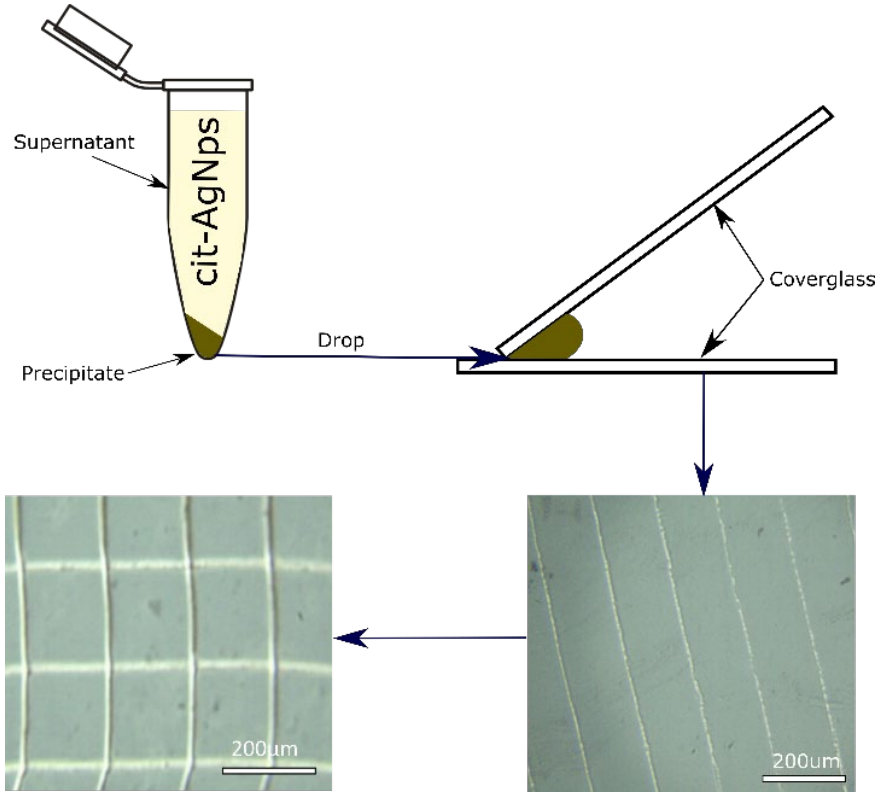

***Figure 2.1**: The workflow of synthesizing silver nanogrid (AgNg) substrates using stop-and-go convective self-assembly (SG-CSA) .*

The morphology of the substrate was optimized in terms of surface-enhanced Raman scattering (SERS) enhancement, using Nile Blue (NB) as test molecule. Therefore, the distance between the AgNWs was varied between 0.05 mm and 0.25 mm. The SERS spectra of 10^{-7} M NB was acquired using the AgNGs with different distances between AgNWs. The limit of detection was tested by varying the NB concentration.

2.2. Surface enhanced-Raman scattering spectra acquisition

2.2.1. Test molecule

SERS spectra were acquired using a Renishaw Raman Spectrometer coupled with a 633 nm laser (0.55 mW power) and a Leica microscope. The AgNGs were immersed in a solution of 10^{-10} M NB, 10^{-4} M $Ca(NO_3)_2$ and 10^{-4} M NaCl for 15 minutes. Then, the substrate was placed onto a microscope slide covered in aluminum foil for the SERS spectra acquisitions.

To optimize the morphology and test the sensitivity of the substrate, the laser was focused onto the substrate using a 5x objective. SERS spectra are represented as a mean of five acquisitions, each three seconds long.

To test the uniformity of the SERS spectra of NB on the AgNWs, an area of 1 mm^2 was mapped. To this regard, the laser was focused onto the substrate using a 100x objective. The SERS spectra were acquired in multiple points with a spatial resolution of 2.5 μm.

The reproducibility of the SERS spectra acquired using the AgNGs was tested on three different substrates.

2.2.2. Serum mixture

SERS spectra were obtained for a serum-mimicking mixture consisting of 10^{-5} M xanthine, 10^{-5} M hypoxanthine, 10^{-5} M creatinine, 10^{-5} M uric acid, 10^{-6} M urea, and 10^{-2} M bovine serum albumin (BSA), utilizing AgNGs as an enhancement substrate.

The AgNGs were immersed in the serum mixture for 15 minutes prior to acquisition. The SERS spectra were collected using a Portable Raman BWTek Plus coupled with a BAC151 Video Microscope, utilizing a 532 nm laser line with a power of 15 mW. Each spectrum was obtained by averaging three acquisitions, each of which lasted for 10 seconds. The SERS spectra were collected from five separate AgNGs substrates, with each substrate yielding five SERS spectra from random distinct points.

2.2.3. Canine serum

SERS spectra of canine serum were collected on both AgNGs substrate and cit-AgNPs substrate. The AgNGs substrate was immersed in a solution of 2 mL ultrapure water containing 20 µL of canine serum and 10^{-4} M of $Ca(NO_3)_2$ for 15 minutes. The SERS spectra were acquired from three randomly selected locations on the substrate. In the case of cit-AgNPs substrate, 90 µL of cit-AgNPs were mixed with 10 µL of canine serum and 10^{-4} M $Ca(NO_3)_2$ and 10^{-4} M NaCl. A 5 µL droplet of the mixture was placed on an aluminum foil-covered microscope slide, and 3 SERS spectra were obtained.

The spectra were collected using a Portable Raman BWTek Plus spectrometer coupled with BAC 151 Video Microscope and a 532 nm laser line (50 mW power). Each spectrum was an average of 3 acquisitions for 10 seconds.

2.2.4. Human serum

To measure SERS spectra of human serum, in colloidal solution of cit-AgNPs we need to deproteineize the human serum. This can be done by simply mixing 900 µL of methanole with 100 µL of serum. After this we use a centrifuge for 15 minutes at 7300 g, at room temperature, then we use the supernatant that is created. This step is done because the protein in the human serum is attracted by the nanoparticles and it makes a corona of protein around the particle, not allowing it to adsorb other molecules, meaning no SERS spectra can be seen.

SERS spectra of human serum were acquired on AgNGs substrate and on cit-AgNPs. The solid substrate was immersed for 15 minutes in a solution of 2 mL ultrapurewater with 20 µL deproteineized human serum. On the colloidal substrate we used 1 mL ultrapurewater with 10 µL deproteineized human serum. On each solution 10^{-4} M $Ca(NO_3)_2$ and 10^{-4} M NaCl was added. Same preparation steps were used for the serum with proteins.

SERS spectra were acquired on the same Portable Raman BWTek Plus spectrometer coupled with BAC 151 Video Microscope, and 532 nm laser (50 mW power). The parameters used for this acquisition are as folowed, for colloidal solution of cit-AgNPs we used 100% power of the laser with 3 acquisitons each for 10 seconds. On the other hand for the solid substrate of AgNGs we used

100% laser power, with 5 acquisition each for 5 seconds 3 times on random spots on the substrate, for 3 substrates.

2.3. SERS spectra processing

The spectral data presented in this manuscript underwent processing using the freely available software Quasar, followed by further refinement in Origin and InkScape to obtain high-quality spectra and figures.

In Origin, the intensity and the Wavenumber data were taken form the .txt file and the spectras were cut from 300 to 1800 cm^{-1} then a rubber band base line correction was applied to each spectra, followed by an area normalization to Peak from 0 (as shwon in Figure 2.3.1). Subsequently, the data was exported to Origin and InkScape for further refinement and optimization of the figures.

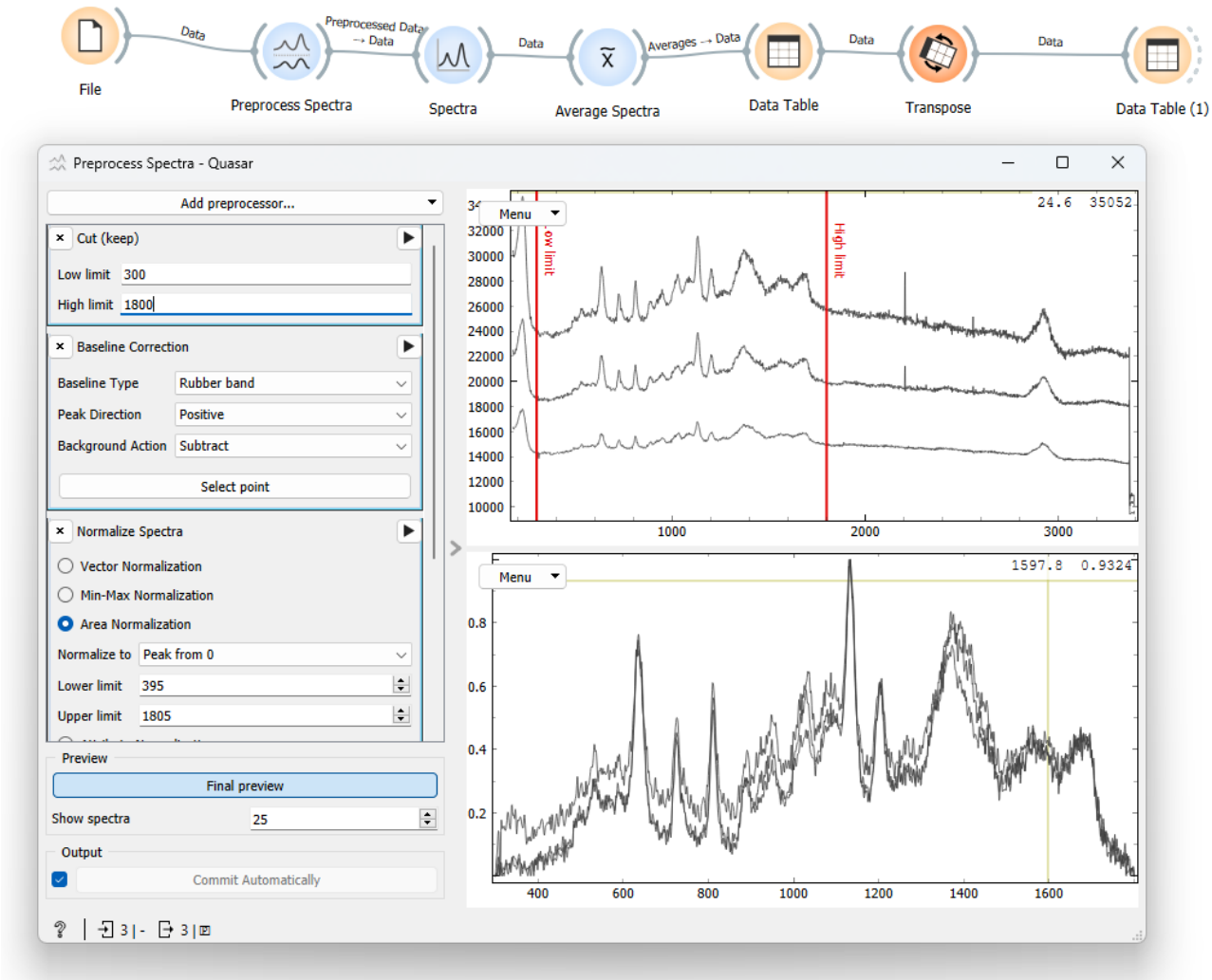

***Figure 2.3**. Quasar spectral processing parameters and workflow.*

2.4. Portable Raman Spectrometer

Figure 2.4. shows the system of portable Raman Spectrometer by B&WTek used in this study, this is equiped with a laser line of 532 nm with a power of 50 mW. The Spectrometer is coupled with a Video Microscope BAC 151 which makes the sample focus possible.

Figure 2.4 B&WTec Portable Raman Spectrosocpe coupled with the BAC 151 Microscope

The spectrometer acquire the spectra in 175-3200 cm^{-1} domain, with a spectral resolution around 4.5 cm^{-1}. The detectio is represented by TE Cooled Lnear Array with 2048 elements of effective detection with a dimension of 14 µm x 200 µm with an integration time between 5-65 ms. [30]

2.5. Renishaw Raman Spectrometer

Figure 2.5. illustrates the Renishaw inVia Raman Spectrometer, a crucial instrument employed in this research. The spectrometer is equipped with a microscope, enabling real-time imaging capabilities, which proves valuable for the study. Of particular significance is its capacity to acquire Raman mapping data. The spectrometer incorporates multiple lasers, providing enhanced spectral resolution by leveraging different laser lines based on the experimental requirements. [31]

Figure 2.5. Renishaw in Via Raman Microscope

2.6. Home-made motorized stage for substrate

Figure 2.6. shows the home made motorized stage used in this study for preparing the AgNG substrate. The equipment used is a ThorLab motorized stage, controled via KBD101 kinesis k-Cube, where a 3D printed support for the cover glass was put on. The 3D printed support has a cut-out with the dimensions of the coverglass used. Another support for the top coverglass whitch was placet at a 40º angle from the first cover glass.

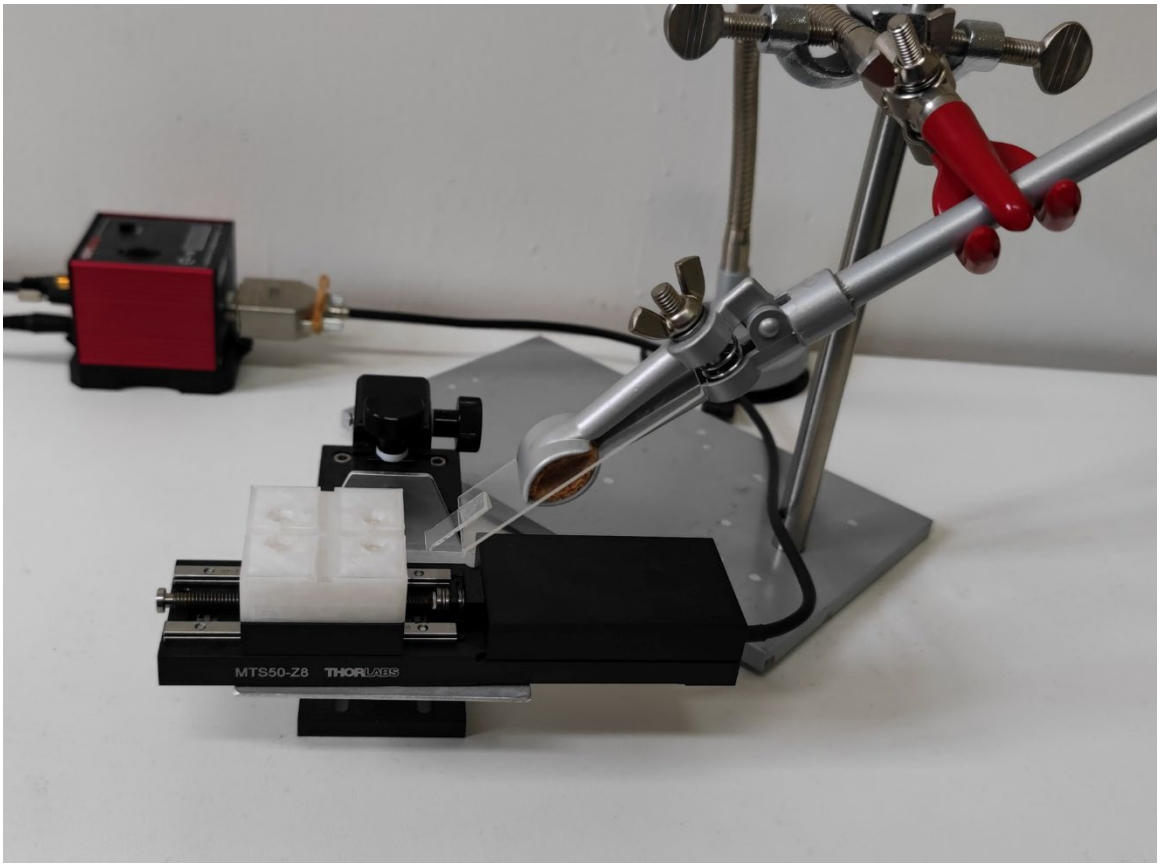

Figure 2.6. Home-Made motorized table.

The unit has a highly compact 60.0 mm x 60.0 mm x 49.2 mm footprint, allowing it to be positioned close to the motorized system for added convenience when manually adjusting motor positions using the top panel controls [32]. Using Thor Labs's Kinesis software, the stage can be moved with a specific acceleration, or a specific velocity. It also can stop at any position, in our case used for the wires of silvernanoparticles to dry on the coverglass.

Chapter 3. Results and discutions

3.1. Optimization of the silver nanogrids (AgNGs) substrate

First, I aimed to investigate the optimal distance between silver nanowires (AgNWs) for surface-enhanced Raman scattering (SERS) spectroscopy. To this regard, I used Nile Blue (NB) as test molecule. AgNWs substrates with varying distances between the wires, ranging from 0.05-0.25 mm, were synthesized and used for acquiring SERS spectra of 10^{-7} M NB. To enhance the SERS signal of NB, the addition of $Ca(NO_3)_2$ and NaCl was necessary for adsorbing NB on the silver surface. All test experiments employed 10^{-4} M $Ca(NO_3)_2$ and 10^{-4} M NaCl mixed with 10^{-7} M NB solutions.

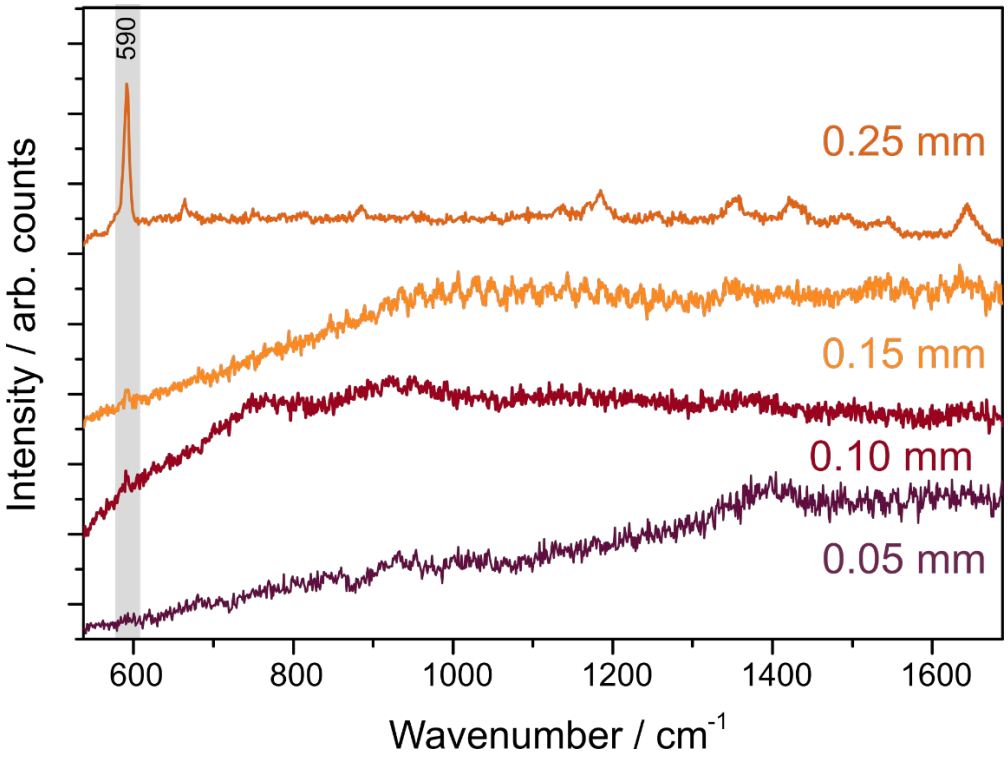

Figure 3.1: SERS spectra of 10^{-7} M Nile Blue (NB) acquired on silver nanogrids (AgNWs) with different distances between the wires ranging from 0.05-0.25 mm.

The results showed that when the distance between the wires was less than 0.25 mm, the SERS spectrum of NB was hardly detectable. However, by increasing the distance between the AgNWs to

0.25 mm, the SERS spectrum of NB became visible. The maximum distance was chosen to ensure that as many wires as possible remained within the field of view.

To increase the surface area covered with silver nanoparticles, the substrate was repeatedly coated with AgNWs, with the second deposition applied perpendicular to the first. Consequently, silver nanogrid substrates (AgNGs) were synthesized, with the distance between the AgNWs set at 0.25 mm. The sensitivity of the AgNGs substrate was assessed by acquiring SERS spectra of NB with varying concentrations, ranging from 10^{-10} to 10^{-7} M. The limit of detection was determined to be 10^{-9} M with a variation of 5.8% between substrates (Figure 3.2). However, lowering the NB concentration to 10^{-10} M resulted in no detectable SERS spectrum.

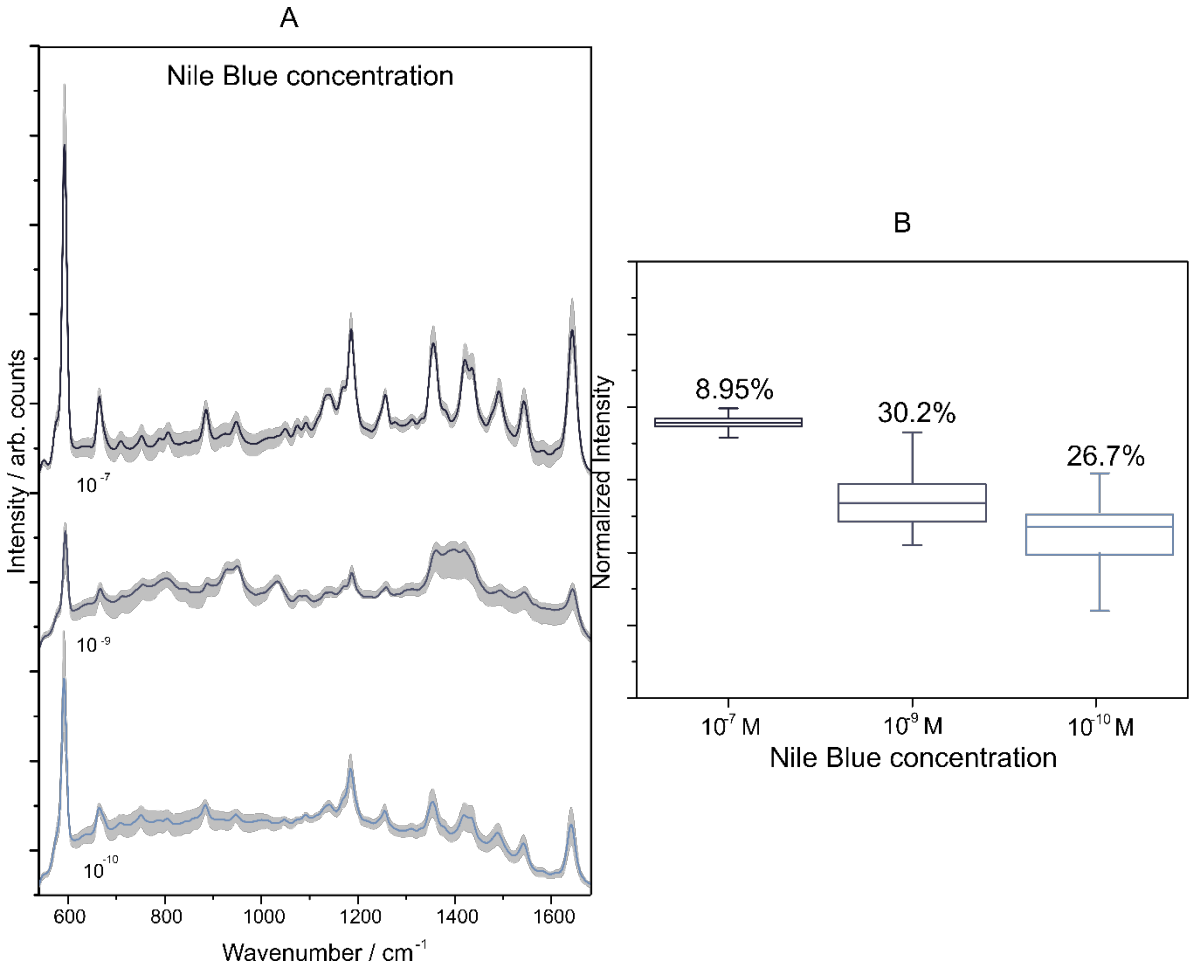

Figure 3.2. *A) Nile Blue SERS spectra at different concentrations of NB. Spectra acquired using Renishaw Raman Spectrometer with a 633 nm laser and a 20x objective, on three solid AgNGs substrates. B) Showing the box plot of the mean standard deviation of the 590 cm^{-1} band from the NB spectra.*

Moreover, the uniformity of the SERS spectra of 10^{-9} M NB was tested on AgNGs, revealing a variation of 6.12% in the acquired SERS signal. Furthermore, a SERS map of an area of 1 mm^2 on the AgNGs was generated (Figure 3.3B). Off the nanogrids, the fluorescence spectrum of the NB was observed, while on the nanogrids, the fluorescence spectrum of NB was quenched due to NB adsorption onto the silver surface, and the SERS spectrum of NB was detected instead (Figure 3.3C).

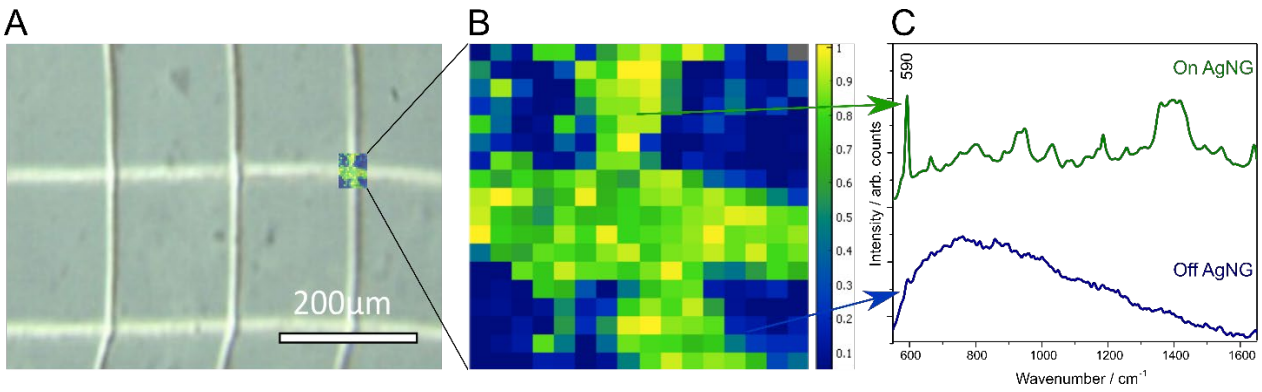

Figure 3.3: *(A) Optical image of silver nanogrids (AgNgs) acquired with an 5x objective (B) Color-encoded mapping of the AgNg represented as the intensity of the SERS band at 590 cm^{-1}, (C) A characteristic SERS spectra of 10^{-9} M Nile Blue acquired on the AgNGs and off the AgNGs.*

3.2. Detection of purine metabolites in the presence of proteins using AgNGs

In order to acquire SERS spectra of serum samples, it is necessary to first remove proteins as they tend to form a protein corona on the surface of the nanoparticles, which obstructs the adsorption of other molecules on the silver surface [33]. However, with AgNGs, the need for protein removal is eliminated, and the SERS spectrum of purine metabolites can be detected even in the presence of albumin.

A serum mixture containing xanthine (10^{-5} M), hypoxanthine (10^{-5} M), creatinine (10^{-5} M), uric acid (10^{-5} M), urea (10^{-6} M), and bovine serum albumin (BSA) (10^{-2} M) was prepared, and the substrate was immersed in the serum mixture to acquire the SERS spectrum. The SERS spectra of the serum mixture exhibited characteristic SERS bands of uric acid (630, 811, 1130, 1200 cm^{-1}), xanthine (1370, 1453 cm^{-1}), and hypoxanthine (722, 1095, 1328, 1580 cm^{-1}). This spectrum is similar to the SERS spectra described in previous literature for mixtures of deproteinized serum and silver colloidal solution.

Additionally, the reproducibility of the SERS spectra of purine metabolites was consistent across five different substrates. The relative mean standard deviation was 20.2% for the 630 cm^{-1} representative peak of xanthine, 20.1% for the 722 cm^{-1} peak attributed to hypoxanthine in literature, 14% for the 1095 cm-1 peak of hypoxanthine, and 4.1% for the 1200 cm^{-1} peak specific to the uric acid molecule.

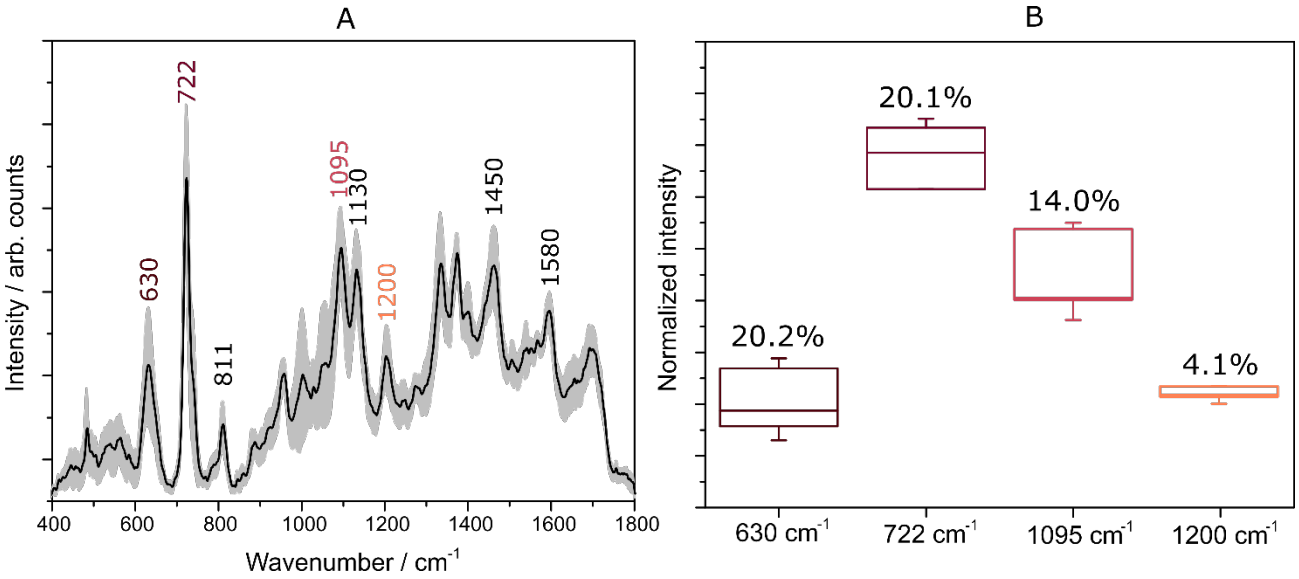

***Figure 3.4**: (A) The SERS spectra of the serum mixture (uric acid, hypoxanthine and xanthine) represented as mean±standard deviation (B) Box plot representation of the intensity of the SERS bandscharacteristic to xanthine, hypoxanthine, and uric acid on five different substrates, showing their variability between substrates.*

The ability to obtain surface-enhanced Raman scattering (SERS) spectra of serum samples on solid silver nanogrids (AgNG) without prior deproteinization was investigated in comparison to using citrate-stabilized silver nanoparticles (cit-AgNPs) in colloidal solutions.

To evaluate this, a canine serum sample was mixed with cit-AgNPs, $Ca(NO_3)_2$, and NaCl, and the resulting SERS spectra were obtained using three separate substrates of solid AgNG and cit-AgNPs. SERS bands of hypoxanthine at 676, 725, and 1335 cm^{-1} were poorly observed in the presence of cit-AgNPs (Figure 3.5, blue spectrum). However, when solid AgNG was used as the metal substrate (Figure 3.5, black spectrum), characteristic SERS bands of purine metabolites were observed at 676, 725, and 1335 cm^{s}. The low variation of the SERS bands of hypoxanthine between the three different substrates, with a standard deviation mean of 12.8%, indicated the reproducibility of the SERS spectra of serum.

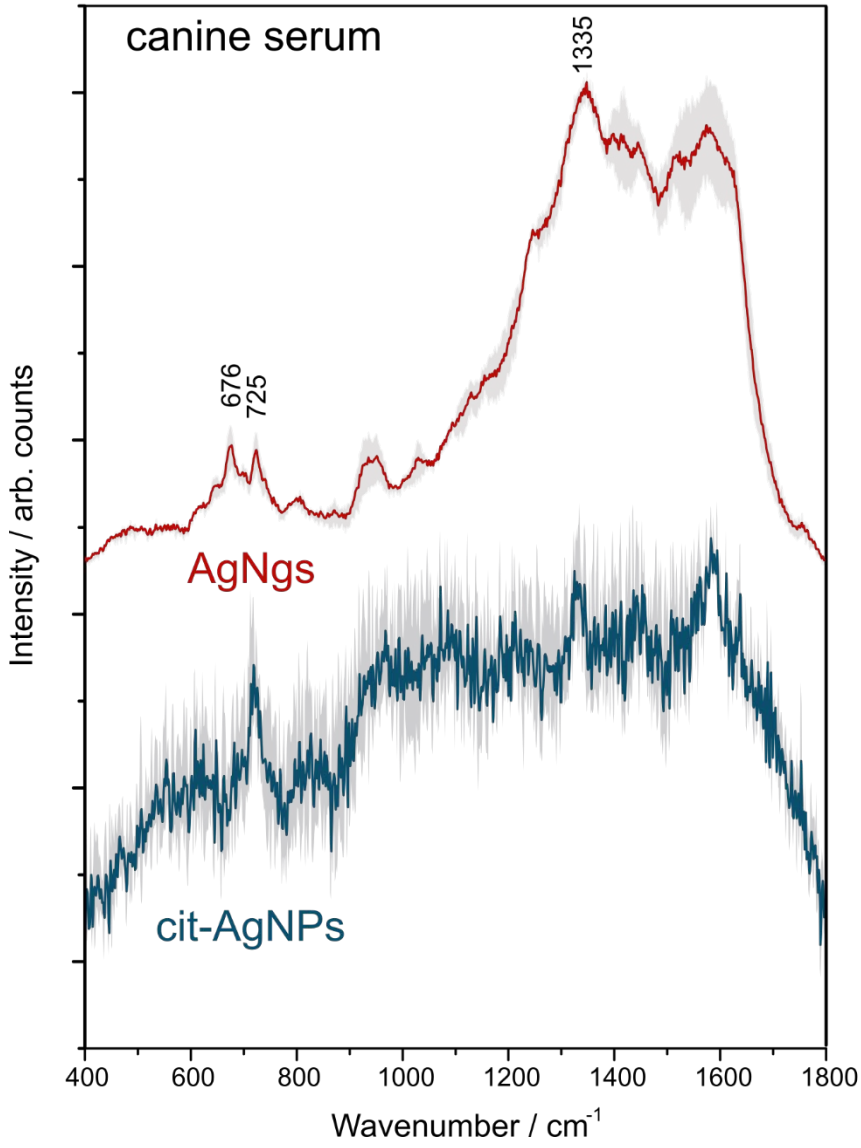

***Figure 3.5**: Mean SERS spectra of canine serum acquired on 3 colloidal solution of cit-AgNPs (blue) and on 3 solid Ag nanogrids substrate (black)*

The subsequent step involved applying the AgNGs substrate to actual human serum samples to assess its comparative efficacy to a basic cit-AgNPs colloidal solution. The results of this investigation are in Figure 3.6 and Figure 3.7, wherein a human serum solution was prepared and subjected to SERS spectroscopy as per the protocols outlined in the materials and methods section.

One initial observation is that the use of either solid AgNGs or colloidal AgNPs as substrates yields a distinct differentiation in proteinated human serum, as evidenced by Figure 3.6. Specifically, when

a colloidal substrate of silver nanoparticles is used (Figure 3.6 blue spectrum), no SERS spectrum is detected. This outcome occurs due to the formation of a protein corona over the nanoparticles, which makes them unable to adsorb additional molecules onto their surfaces [33]. However, when a solid substrate is used (Figure 3.6 red spectrum), bands corresponding to purine metabolites such as uric acid (630, 811, 1133, and 1200 cm^{-1}) and hypoxanthine (722 and 1095 cm^{-1}) are discernible.

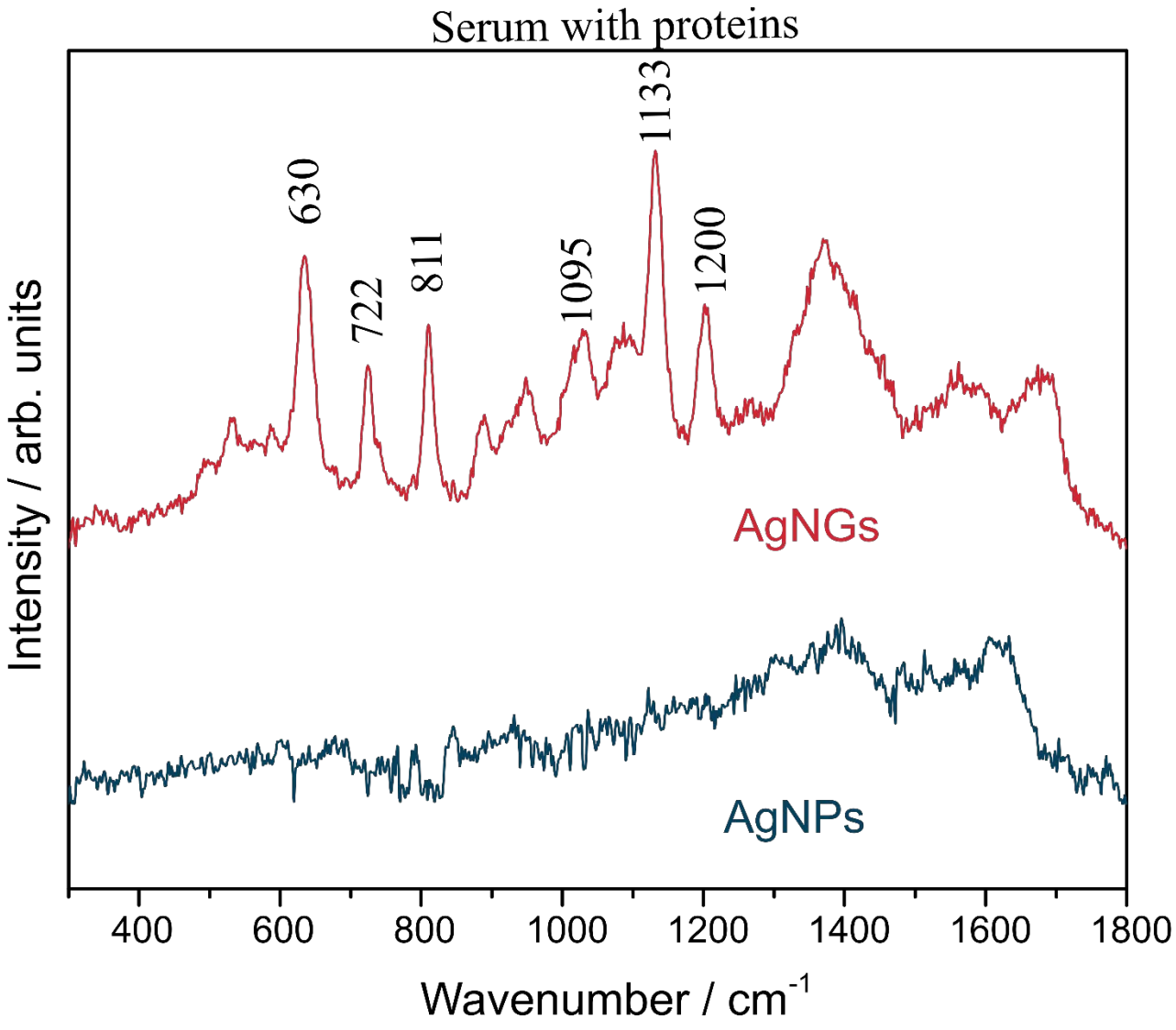

***Figure 3.6**: Mean spectrum of human serum with proteins, SERS acquisition (blue) using AgNPs on 3 different substrates, (red) using AgNGs on 3 different substrates.*

The subsequent observation involved a comparison of the SERS spectra acquired from proteinized human serum on solid AgNGs substrate (Figure 3.7 red spectra) to those obtained from deproteinized human serum on colloidal AgNPs substrate (Figure 3.7 blue spectra), with discernible variations in band intensity observed between them. However, the overall profiles of the spectra were found to be identical.

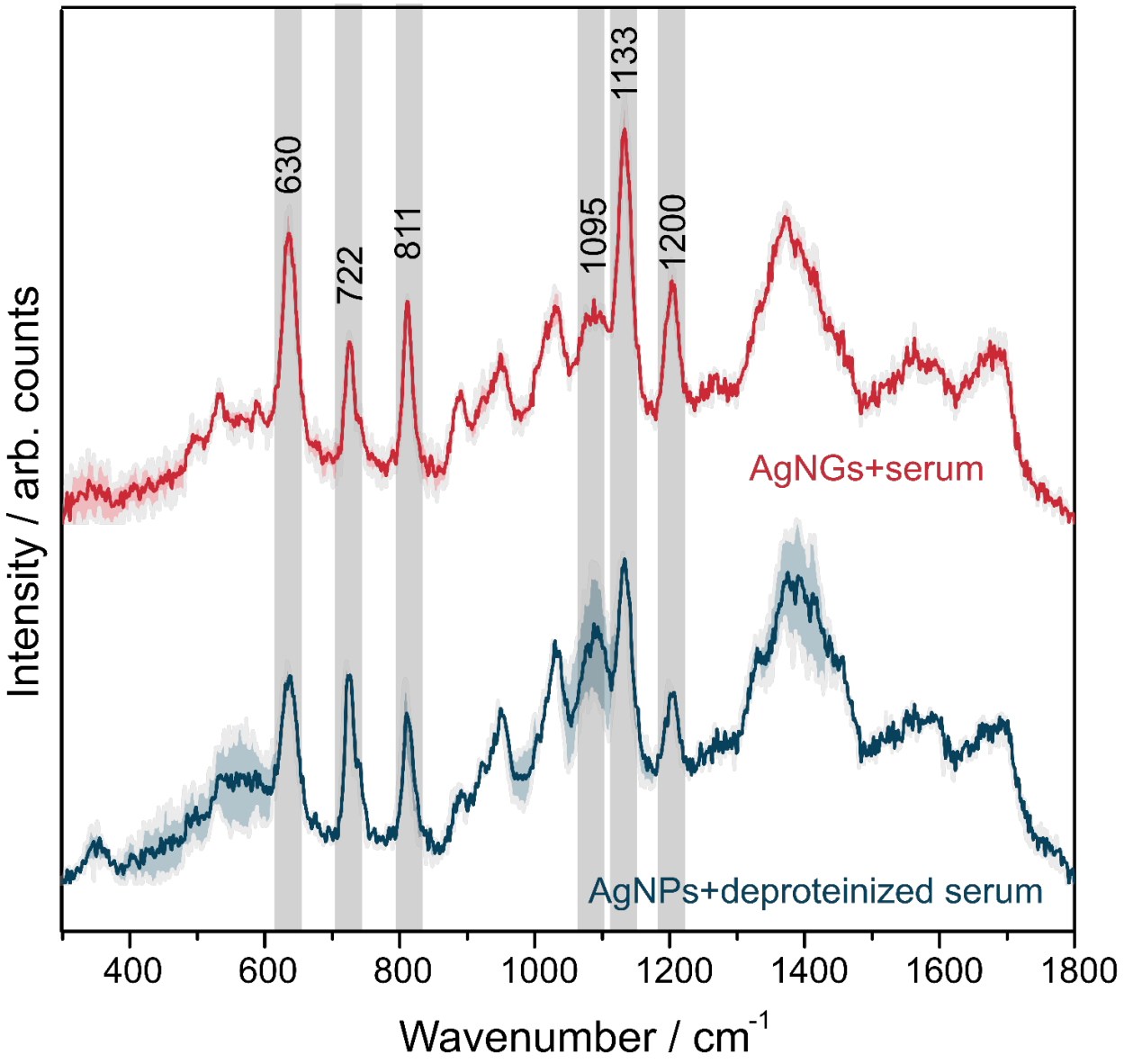

Figure 3.7: Mean spectrum of human serum, which was deproteinized for SERS acquisition (blue) using AgNPs on 3 different substrates, and proteinized serum SERS spectra (red) using AgNGs on 3 different substrates.

Conclusions

In conclusion this study is highilting the potential of solid substrates for Surface Enhanced Raman Spectroscopy (SERS) spectra of canine and human serum samples without the need for a deproteinization step, by optimizing a new solid substrate called silver nanogrids (AgNGs). The AgNGs substrate's performance was evaluated using Nile Blue (NB), and it was determined that the lowest detectable concentration of NB was 10^{-9} M. The optimal distance between the wires of the substrate was found to be 0.25 mm. The SERS spectra varied by 6.17% along the wires, while the difference between substrates was 5.8%.

Additionally, it was demonstrated that AgNGs can detect purine metabolites in the presence of proteins, unlike when using a colloidal solution of silver nanoparticles which requires a deproteinization step. SERS spectra were acquired using five different AgNGs substrates, and reproducibility was confirmed by obtaining spectra from five random positions on each substrate with low variation in the SERS signal.

When AgNGs substrate was used with canine and human samples in the presence of proteins, SERS spectra of purine metabolites were obtained, whereas using colloidal silver nanoparticles solutions without deproteinization resulted in no SERS spectra.

The optimized AgNGs substrate shows great potential for clinical applications in SERS, particularly in detecting purine metabolites in serum with low concentrations and in the presence of proteins. Further research can explore the substrate's potential with other real-world samples and biomolecules.

References

1. Cialla D, März A, Böhme R, et al (2012) Surface-enhanced Raman spectroscopy (SERS): progress and trends. Anal Bioanal Chem 403:27–54. https://doi.org/10.1007/s00216-011-5631-x

2. Zou Y, Huang M, Wang K, et al (2016) Urine surface-enhanced Raman spectroscopy for non-invasive diabetic detection based on a portable Raman spectrometer. Laser Phys Lett 13:065604. https://doi.org/10.1088/1612-2011/13/6/065604

3. Zong C, Xu M, Xu L-J, et al (2018) Surface-Enhanced Raman Spectroscopy for Bioanalysis: Reliability and Challenges. Chem Rev 118:4946–4980. https://doi.org/10.1021/acs.chemrev.7b00668

4. Avci E, Yilmaz H, Sahiner N, et al (2022) Label-Free Surface Enhanced Raman Spectroscopy for Cancer Detection. Cancers 14:5021. https://doi.org/10.3390/cancers14205021

5. Esposito A, Bonifacio A, Sergo V, Fornasaro S (2021) Label-free Surface Enhanced Raman Scattering (SERS) on Centrifugal Silver Plasmonic Paper (CSPP): A Novel Methodology for Unprocessed Biofluids Sampling and Analysis. Biosensors 11:467. https://doi.org/10.3390/bios11110467

6. Moisoiu V, Iancu SD, Stefancu A, et al (2021) SERS liquid biopsy: An emerging tool for medical diagnosis. Colloids Surf B Biointerfaces 208:112064. https://doi.org/10.1016/j.colsurfb.2021.112064

7. Yang B, Jin S, Wang Y, et al (2019) Disease-related proteins determination based on surface-enhanced Raman spectroscopy. Applied Spectroscopy Reviews 54:856–872. https://doi.org/10.1080/05704928.2018.1557676

8. Li J, She Q, Wang W, et al (2023) Label-Free SERS Analysis of Serum Using Ag NPs/Cellulose Nanocrystal/Graphene Oxide Nanocomposite Film Substrate in Screening Colon Cancer. Nanomaterials 13:334. https://doi.org/10.3390/nano13020334

9. Farcau C, Sangeetha NM, Moreira H, et al (2011) High-Sensitivity Strain Gauge Based on a Single Wire of Gold Nanoparticles Fabricated by Stop-and-Go Convective Self-Assembly. ACS Nano 5:7137–7143. https://doi.org/10.1021/nn201833y

10. Freeman RG, Grabar KC, Allison KJ, et al (1995) Self-Assembled Metal Colloid Monolayers: An Approach to SERS Substrates. Science 267:1629–1632. https://doi.org/10.1126/science.267.5204.1629

11. Thurn-Albrecht T, Schotter J, Kästle GA, et al (2000) Ultrahigh-Density Nanowire Arrays Grown in Self-Assembled Diblock Copolymer Templates. Science 290:2126–2129. https://doi.org/10.1126/science.290.5499.2126

12. Garcia MA (2011) Surface plasmons in metallic nanoparticles: Fundamentals and applications. Journal of Physics D: Applied Physics 44:283001. https://doi.org/10.1088/0022-3727/44/28/283001

13. Kraus T, Malaquin L, Delamarche E, et al (2005) Closing the Gap Between Self-Assembly and Microsystems Using Self-Assembly, Transfer, and Integration of Particles. Advanced Materials 17:2438–2442. https://doi.org/10.1002/adma.200501171

14. Prevo BG, Kuncicky DM, Velev OD (2007) Engineered deposition of coatings from nano- and micro-particles: A brief review of convective assembly at high volume fraction. Colloids and Surfaces A: Physicochemical and Engineering Aspects 311:2–10. https://doi.org/10.1016/j.colsurfa.2007.08.030

15. Leopold N (2009) Surface-enhanced Raman Spectroscopy: Selected Applications. Napoca Star

16. Fortin T, Salvador A, Charrier JP, et al (2009) Clinical quantitation of prostate-specific antigen biomarker in the low nanogram/milliliter range by conventional bore liquid chromatography-tandem mass spectrometry (multiple reaction monitoring) coupling and correlation with ELISA tests. Mol Cell Proteomics 8:1006–1015. https://doi.org/10.1074/mcp.M800238-MCP200

17. Moskovits M (1979) Enhanced Raman scattering by molecules adsorbed on electrodes--a theoretical model. Solid State Communications 32:59–62. https://doi.org/10.1016/0038-1098(79)90997-9

18. Moskovits M (1985) Surface-enhanced spectroscopy. Rev Mod Phys 57:783–826. https://doi.org/10.1103/RevModPhys.57.783

19. Liang J, Liu H, Yu J, et al (2019) Plasmon-enhanced solar vapor generation. Nanophotonics 8:771–786. https://doi.org/10.1515/nanoph-2019-0039

20. Muniz-Miranda M, Muniz-Miranda F, Pedone A (2018) Spectroscopic and Computational Studies on Ligand-Capped Metal Nanoparticles and Clusters. In: Deepak FL (ed) Metal Nanoparticles and Clusters. Springer International Publishing, Cham, pp 55–87

21. Boerigter C, Aslam U, Linic S (2016) Mechanism of Charge Transfer from Plasmonic Nanostructures to Chemically Attached Materials. ACS Nano 10:6108–6115. https://doi.org/10.1021/acsnano.6b01846

22. Ru EL, Etchegoin P (2008) Principles of Surface-Enhanced Raman Spectroscopy: and Related Plasmonic Effects. Elsevier

23. Lombardi J, Birke R (2008) A Unified Approach to Surface-Enhanced Raman Spectroscopy. Journal of Physical Chemistry C - J PHYS CHEM C 112:. https://doi.org/10.1021/jp800167v

24. Kudelski A, Bukowska J (1996) The chemical effect in surface enhanced Raman scattering (SERS) for piperidine adsorbed on a silver electrode. Surface Science 368:396–400. https://doi.org/10.1016/S0039-6028(96)01082-5

25. Kong KV, Leong WK, Lam Z, et al (2014) A Rapid and Label-free SERS Detection Method for Biomarkers in Clinical Biofluids. Small 10:5030–5034. https://doi.org/10.1002/smll.201401713

26. Bonifacio A, Cervo S, Sergo V (2015) Label-free surface-enhanced Raman spectroscopy of biofluids: fundamental aspects and diagnostic applications. Anal Bioanal Chem 407:8265–8277. https://doi.org/10.1007/s00216-015-8697-z

27. Lundqvist M, Stigler J, Cedervall T, et al (2011) The Evolution of the Protein Corona around Nanoparticles: A Test Study. ACS Nano 5:7503–7509. https://doi.org/10.1021/nn202458g

28. Fathallah-Shaykh SA, Cramer MT (2014) Uric acid and the kidney. Pediatr Nephrol 29:999–1008. https://doi.org/10.1007/s00467-013-2549-x

29. Lee PC, Meisel D (1982) Adsorption and surface-enhanced Raman of dyes on silver and gold sols. J Phys Chem 86:3391–3395. https://doi.org/10.1021/j100214a025

30. Portable Raman Spectrometer with High Sensitivity – i-Raman Plus®. https://bwtek.com/products/i-raman-plus/. Accessed 10 May 2023

31. plc R Renishaw: inVia confocal Raman microscope. In: Renishaw. http://www.renishaw.com/en/invia-confocal-raman-microscope--6260. Accessed 21 May 2023

32. Kinesis® K-Cube™ Brushless DC Servo Controller. https://www.thorlabs.com. Accessed 10 May 2023

33. Jahan Sajib MS, Sarker P, Wei Y, et al (2020) Protein Corona on Gold Nanoparticles Studied with Coarse-Grained Simulations. Langmuir 36:13356–13363. https://doi.org/10.1021/acs.langmuir.0c02767

Anexa 1.

DECLARAȚIE PE PROPRIE RĂSPUNDERE

Subsemnatul, Chiș Alexandru Ștefan, declar că Lucrarea de licență/diplomă/disertație pe care o voi prezenta în cadrul examenului de finalizare a studiilor la Facultatea de Fizică, din cadrul Universității Babeș-Bolyai, în sesiunea iulie 2023 , sub îndrumarea Prof. Dr. Nicolae Leopold, reprezintă o operă personală. Menționez că nu am plagiat o altă lucrare publicată, prezentată public sau un fișier postat pe Internet. Pentru realizarea lucrării am folosit exclusiv bibliografia prezentată și nu am ascuns nici o altă sursă bibliografică sau fișier electronic pe care să le fi folosit la redactarea lucrării.

Prezenta declarație este parte a lucrării și se anexează la aceasta.

Data,

Nume,

Chiș Alexandru Ștefan

Semnătură